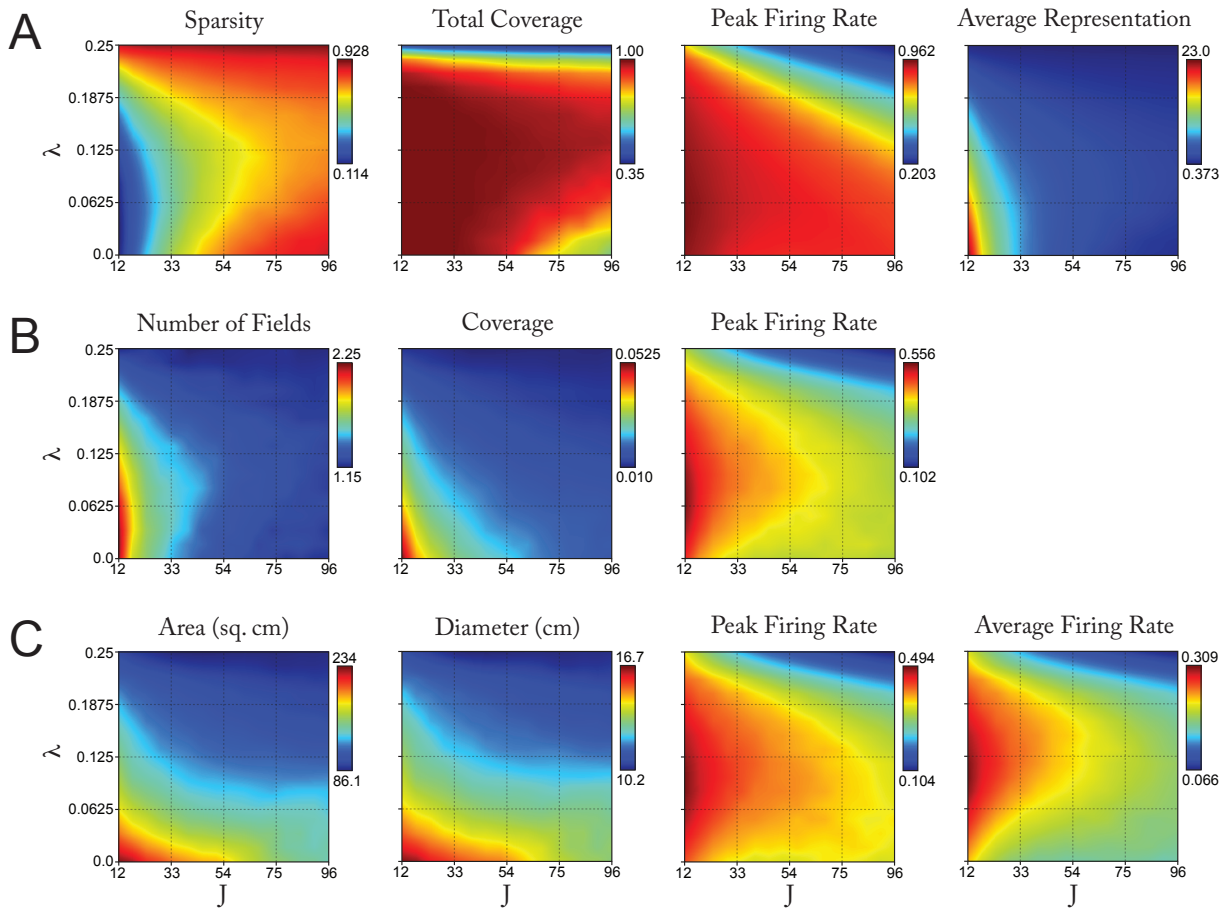

Figure S1. **The competitive parameter dependence of spatial map, place unit, and place field characteristics.** The measures computed here are based on the same 16×16 parameter sweep of inhibitory strength J and threshold λ shown in Figure 4. The sparsity (A), number of fields and peak firing rate (B), and area (C) plots are the same panels shown in Figure 4. The 11 measures shown here (in three categories) are the same used to quantify the sample sets summarized in Table 1. **A.** Spatial map values (left to right): network sparsity (proportion of inactive units), coverage (proportion of environment overlapped by at least one place field), peak firing rate of strongest place unit, and average representation (average number of place fields overlapping a given point in the environemt). **B.** Active place unit values (l to r): number of place fields, coverage (including primary and secondary place fields), and peak firing rate. **C.** Place field values (l to r): area, diameter (computed directly from area, assuming place field circularity), peak firing rate, and average rate across the extent of the place field. Spatial coding measures based on field size (representation, place unit coverage, area) are monotonic decreasing with J and λ; other measures are non-monotonic in λ depending on the strength of inhibition.

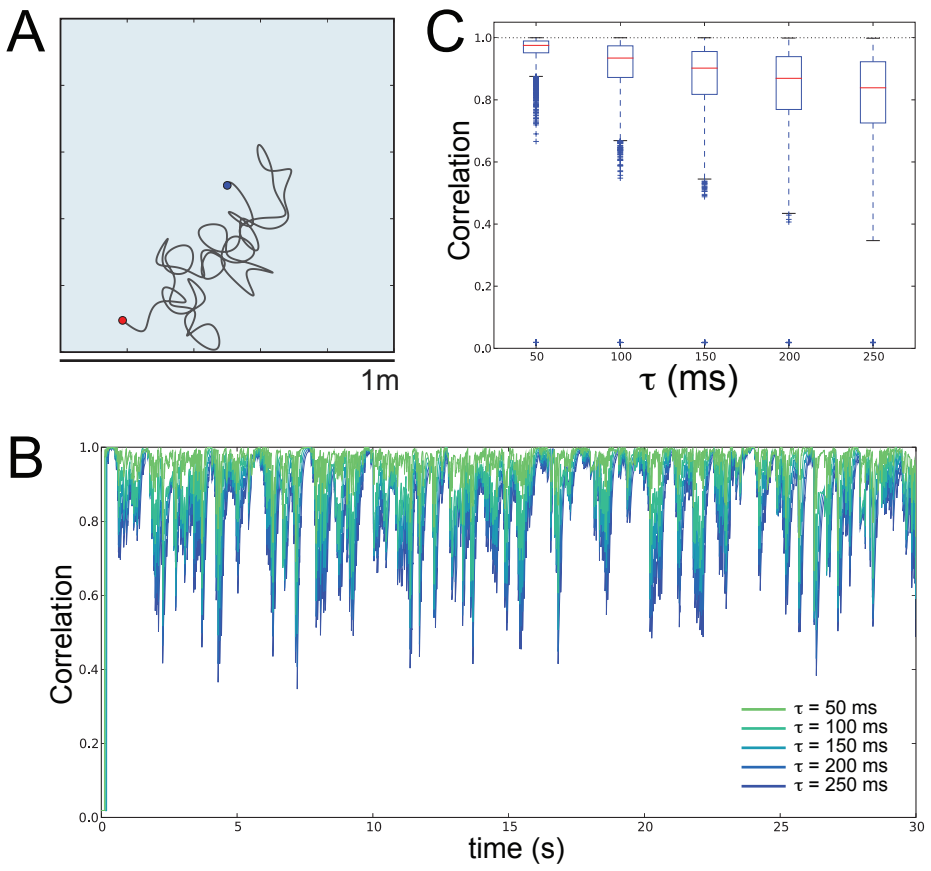

Figure S2. **Spatial responses determined using an artificial raster trajectory are strongly correlated with responses to a naturalistic trajectory.** We simulated the spatial map for a single grid/place-network pair as usual (Methods) and compared it to the real-time output of a smoothed random-walk trajectory (average speed 15 cm/s). **A.** The 30-s trajectory through the 1 sq. m. environment (blue circle: start location; red circle: end location). **B.** Correlation strength between corresponding population rates in the raster-scan spatial map and the random-walk responses across time. The naturalistic trajectory was simulated with five different values for the integration time-constant τ (Equation 3), ranging from 50–250 ms. **C.** Box-and-whiskers plots of the distribution of trajectory correlations across time for each τ.

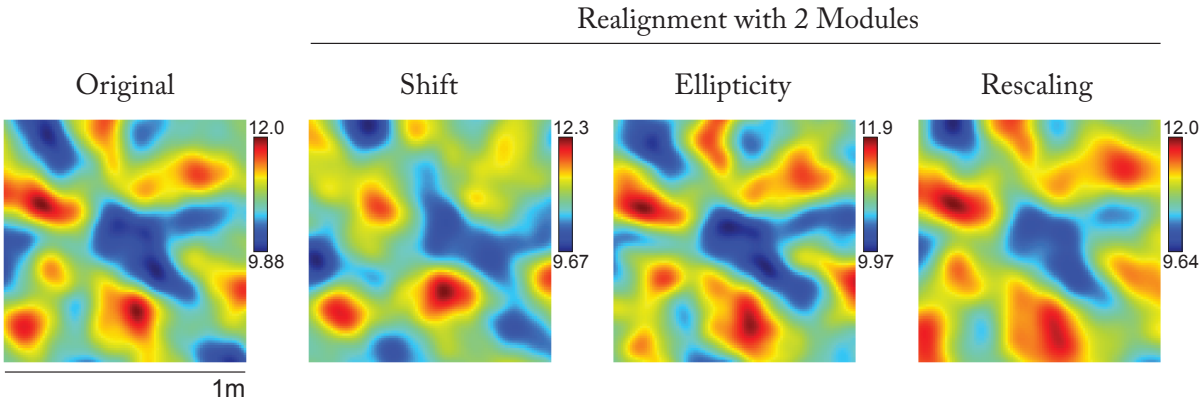

Figure S3. **Spatial modulation of afferent excitatory drive from the population of simulated grid inputs is modified by modular realignment.** For each pixel in the environment, we compute the magnitude of the population rate vector of the grid responses (Equation 1). The spatial modulation of excitation due to the original environment A (left) used for the realignment examples (Figure 5) shows several distinct peaks and valleys [cf. Figure 5 of Almeida et al. (2009) *J Neurosci*, *29*(23), 7504–7512]. The three realignments using two random modules have varying effects on the distribution of excitation across the environment (three right panels). With just two independently realigning modules, the relative effects of realignment on the spatial distribution of excitation are apparent from visual inspection.

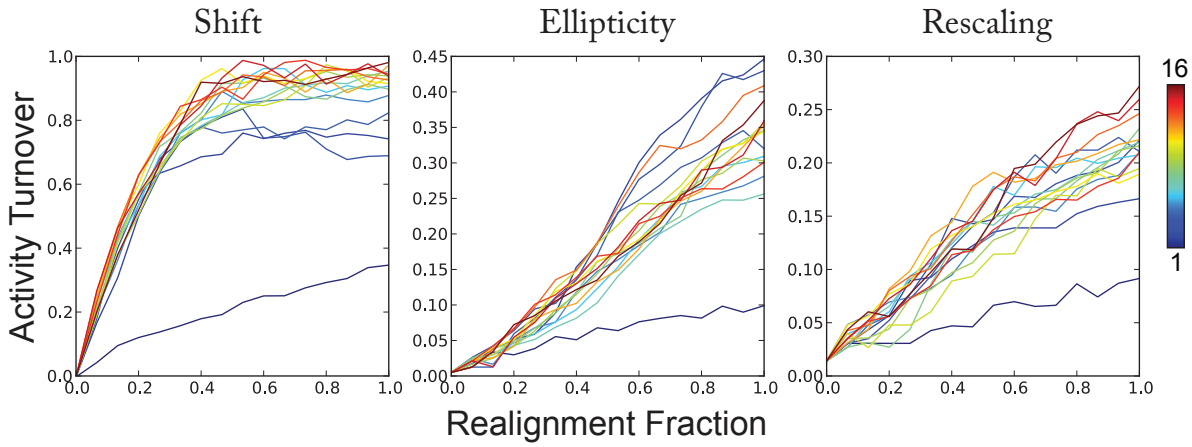

Figure S4. **Activity turnover during progressive modular remapping as inputs are realigned between two environments.** For the same randomly sampled realignments across varying degrees of modularity as in Figure 6B, these panels present the measure of activity turnover. The trends and relative magnitudes between realignments for turnover are qualitatively similar to those observed for the measure of remapping strength. The gradual increase of turnover with increasing modularity in the shift realignment is more consistent than the analogous increase of remapping strength.

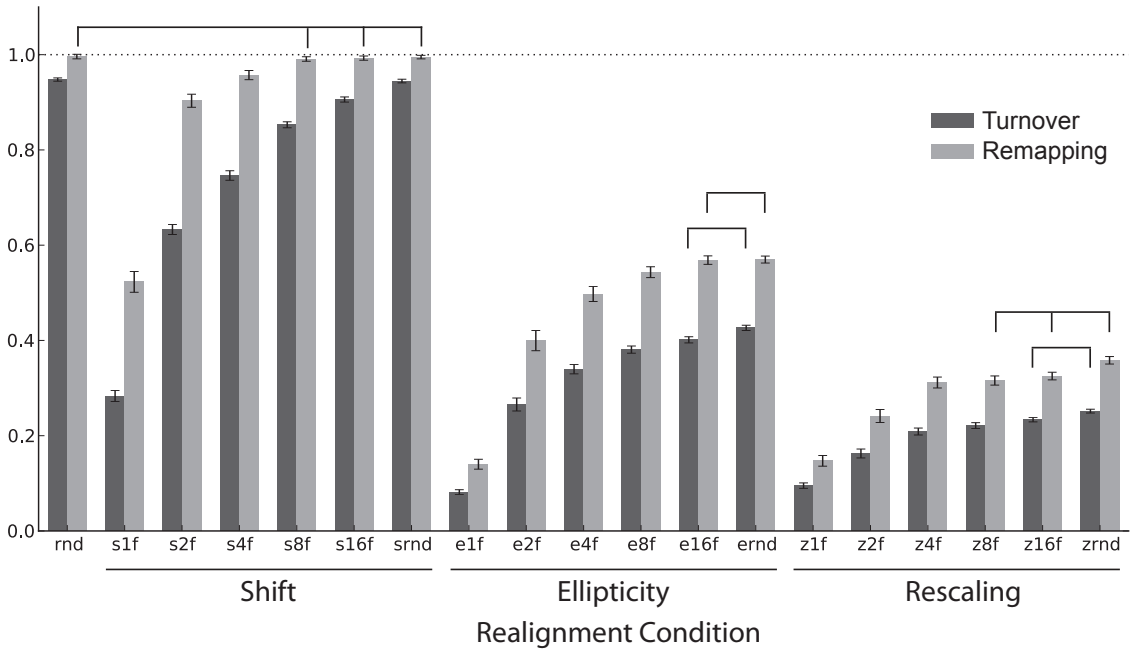

Figure S5. **Statistics computed on sets of 64 remapping simulations using spatial frequency modules.** The same realignment conditions presented in Figure 7a were simulated using frequency modules as opposed to random modules (Methods). The *rnd*, *srnd*, *ernd*, and *zrnd* data are the same sample sets from Figure 7a, as those conditions are equivalent between module types. Data are presented similarly here (bars and error bars show means $\pm$ s.e.m., Horizontal bars indicate the two-sample K–S test is not significant at $p > 0.05$). These means are used for the module type comparisons in Figure 7b and c. For both ellipticity and rescaling, 16 modules are necessary for realignment to not significantly differ from the incoherent conditions *ernd* and *zrnd*, respectively.